Lubricant-Infused Nanoparticulate Coatings Assembled by Layer-by-Layer Deposition

DOI: 10.1002/ ((please add manuscript number))
Article type: Full Paper

Lubricant-infused Nanoparticulate Coatings Assembled by Layer-by-layer Deposition

Steffi Sunny,[1,§] Nicolas Vogel,[1,§,] Caitlin Howell,[1,2] Thy L. Vu[1,2] and Joanna Aizenberg[1,2,3,*]*

[1]School of Engineering and Applied Sciences, Harvard University, Cambridge, MA 02138, USA

[2]Wyss Institute for Biologically Inspired Engineering, Harvard University, Cambridge, MA 02138, USA

[3]Department of Chemistry and Chemical Biology, Harvard University, Cambridge, MA 02138, USA

*To whom correspondence should be addressed. Email: jaiz@seas.harvard.edu, nvogel@seas.harvard.edu

[§]Authors contributed equally

Keywords: colloids, layer-by-layer, nanostructures, wetting, omniphobicity

Abstract:

Omniphobic coatings are designed to repel a wide range of liquids without leaving stains on the surface. A practical coating should exhibit stable repellency, show no interference with color or transparency of the underlying substrate and, ideally, be deposited in a simple process on arbitrarily shaped surfaces. We use layer-by-layer (LbL) deposition of negatively charged silica nanoparticles and positively charged polyelectrolytes to create nanoscale surface structures that are further surface-functionalized with fluorinated silanes and infiltrated with fluorinated oil, forming a smooth, highly repellent coating on surfaces of different materials and shapes. We show that four or more LbL cycles introduce sufficient surface roughness to effectively immobilize the lubricant into the nanoporous coating and provide a stable liquid

interface that repels water, low-surface-tension liquids and complex fluids. The absence of hierarchical structures and the small size of the silica nanoparticles enables complete transparency of the coating, with light transmittance exceeding that of normal glass. The coating is mechanically robust, maintains its repellency after exposure to continuous flow for several days and prevents adsorption of streptavidin as a model protein. The LbL process is conceptually simple, of low cost, environmentally benign, scalable, automatable and therefore may present an efficient synthetic route to non-fouling materials.

1. Introduction

A self-cleaning coating that repels various contaminating liquids without staining the substrate will impact a wide range of technological and consumer applications, including surface coatings on windows, lenses or solar cells, repellent or protective clothing, non-fouling marine vessels or biomedical devices, and anti-icing or drag-reducing surfaces. An ideal coating should ensure stable repellency, should be transparent in order not to affect color or transparency of the underlying substrate and should be able to be deposited in a simple process on materials regardless of their size, shape, or composition. The key difficulty in creating such omniphobic coatings is to overcome the strong tendency of low-surface-tension organic liquids to wet surfaces[1-2] and the adsorption of organic contaminants (especially proteins, cells or bacteria) that can compromise the repellent properties.[3-5]

Traditional superhydrophobic surface designs are inspired by the lotus leaf[6] and rely on the creation of air-infused micro/nanostructured surfaces to minimize the contact points between the liquid to be repelled and the substrate.[7-10] The best of them outperform the lotus leaves due to sophisticated hierarchical structuration, designed to repel low-surface-tension liquids,[1-2, 11] enable repellency under water[12] or control the movement of water droplets.[13-14] However, these structures often rely on complex re-entrant geometries to achieve repellency, which can require involved preparation protocols.

An experimentally simple layer-by-layer assembly method of polyelectrolyte and nanoparticle layers to create superhydrophobic coatings was previously presented as a possible solution to avoid complex fabrication.[15-17] Originating from the technique established by Decher *et al*[18-19] these assemblies can be made with ease and applied to surfaces of various materials, sizes, and shapes, making them useful for many applications.[20-28] While the simplicity of the method offers a solution to the practical limitations of more complex designs of surface topography, the fundamental issues associated with lotus leaf-mimicking materials remain. The composite solid/air interface in the superhydrophobic, lotus leaf inspired design is metastable. The air layer can escape the structures upon damage, application of low-surface-tension liquids, under pressure or at elevated temperature, leading to failure of the coating.

An alternative approach for creating repellent coatings is lubricant-infused micro/nanostructured surfaces that derive their performance from a stable *liquid* film formed at the interface.[8,29-31] In lubricant-infused materials, the functionalized, structured solid immobilizes a fluid lubricant layer on the substrate, producing a thermodynamically stable solid/lubricant interface when roughness, surface chemistry and lubricant are properly matched.[30] This immobilized lubricant layer effectively prevents any test liquid from being in contact with the underlying solid substrate and consequently, reduces pinning. As a result, the test liquid is easily shed from the surface. The elimination of direct contact between the liquid and the solid substrate also prevents adhesion of liquid-borne contaminants including bacteria[32-33] and drastically lowers the adhesion of ice.[34-36] The liquid nature of the lubricant introduces further benefits, such as self-healing properties,[30,37] pressure and temperature stability,[38-39] enhanced condensation[40] and heat transfer,[41] and dynamic control of the wettability.[37]

This fast developing area has led to different approaches of introducing roughness features on various substrates. Lubricant-infused slippery surfaces can be simply formed

using porous membranes[30,37] where thermodynamically stable lubricant films enable excellent repellency. However, difficulties associated with the attachment of such porous membranes to various types of substrates limit their practical applications. Similarly, micron-scale topography can be introduced via photolithography but this technique limits the ability to cover curved surfaces.[30, 40] Electrochemical deposition,[34] and porous polymer films[33,42] also achieve thermodynamically stable lubricant films; however, the coating is substrate-dependent and generally lacks transparency. Sol-gel approaches[43-44] allow transparency of the coating but usually lack mechanical stability. A closed-cell nanoscale architecture prepared from colloidal templating has been shown to be mechanically robust but is limited in scalability and cannot be applied to more complex substrates, for example the inside of tubes or pipes.[45] While all of these recent innovations have tremendously increased scope and applicability of lubricant-infused coatings, the need remains to establish an experimentally simple and versatile coating method.

Since the underlying solid structure simply serves to facilitate wetting of the lubricant into the surfaces features (*i.e.* creating a Wenzel state[46] for the lubricant) instead of preventing the wetting of the liquid to be repelled (*i.e.* creating metastable Cassie Baxter states[47]), one can employ virtually any method to create surface roughness. LbL assemblies, characterized by ease of applicability to various surfaces of arbitrary shapes, scalability and the possibility of automation are a promising starting point when seeking a simple yet powerful coating method. Recently, Zacharia *et al* recognized the potential of this method to create lubricant-infused, repellent surfaces.[48] They used LbL to prepare a hierarchical coating consisting of a micron-sized porous polyelectrolyte multilayer architecture decorated with silica nanoparticles. As expected, the process allows application of the repellent coating on arbitrarily-shaped surfaces with high homogeneity. However, their protocol, involving hierarchical structuration increases the total thickness of the coating and therefore impedes transparency. Furthermore, it has been shown that plain polyelectrolyte multilayer films are

mechanically feeble and require additional modifications (i.e. chemical crosslinking) to acquire wear resistance.[49]

To overcome these issues, we adopt an experimentally simple LbL deposition of silica nanoparticles[15, 17, 50] to create a lubricant-infused *nanoscale* coating with high transparency and good mechanical robustness. Positively charged polyelectrolytes and negatively charged silica nanoparticles are assembled onto a given substrate, sintered at high temperature, surface modified by silane chemistry, and infused with a lubricant matching in chemical composition. The small size of the silica nanoparticles results in a nanoscale film that supports effective liquid repellency without any further structural hierarchy, thus preventing unwanted scattering of light at larger roughness features, leading to complete transparency of the coating. Yet, it can create a sufficiently rough interface to stably entrap the lubricant to form a smooth liquid overlayer that repels a second immiscible liquid. Previously, we have found that the absence of hierarchy indeed increases the performance of lubricant-infused coatings.[43] The sintering of the colloidal layers at elevated temperatures further creates a more robust interconnected network of particles,[51] which significantly reduces the coating's susceptibility to mechanical damage, which we assess by tape peel tests. This method allows us to combine a multitude of desirable properties including liquid repellency, transparency, mechanical stability, and antifouling properties with the appealing characteristics of the LbL coating approach, such as process automation, scalability, and application to glass surfaces of various shapes. Different substrate materials can be coated as well, given that they can be treated with oxygen plasma to activate the surface.

2. Results and Discussion

Coating process. **Figure 1** schematically shows the fabrication of the surface coating. In brief, negative charges are created on the substrate by plasma treatment, UV-ozone or immersion in base piranha solution. The substrate is subsequently immersed into a solution of

positively charged polyelectrolyte (poly-diallyldimethyl ammonium chloride, PDADMAC), rinsed and immersed into a solution of negatively charged Ludox™ silica nanoparticles.[15, 17, 50] Electrostatic attraction leads to the formation of a fuzzy, disordered film of polymer and nanoparticles.[18-19] The alternate deposition of PDADMAC and silica particles is repeated multiple times, as desired. The assembled hybrid film is calcined or plasma-treated to remove the polymer and to activate the silica nanoparticle surfaces, leaving a disordered, porous silica nanoparticle assembly on the substrate, the surface of which is subsequently silanized with 1H,1H,2H,2H-(tetrahydrotridecafluorooctyl)-trichlorosilane to produce a fluorinated surface. A fluorinated lubricant oil (DuPont Krytox™ 100), matching the surface chemistry of the coating, is then infiltrated into the porous structure to create a thermodynamically stable, immobilized lubricant layer that prevents a second, immiscible liquid from contacting and pinning on the underlying solid, thus creating a slippery, lubricant-infused porous surface (SLIPS).[30]

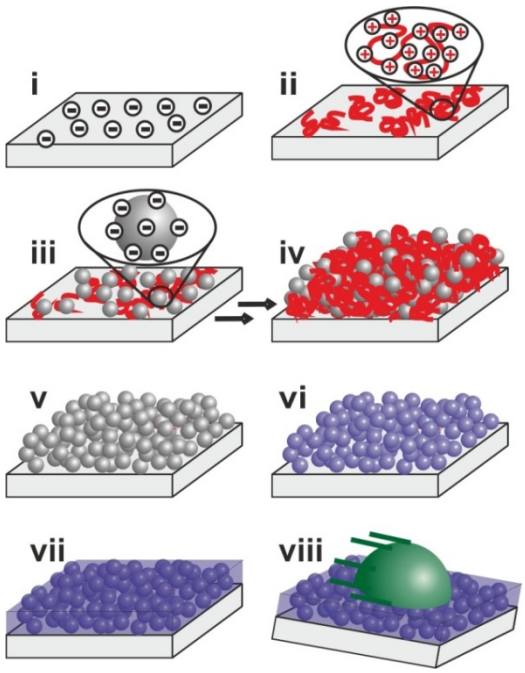

Figure 1. Schematic illustration of the layer-by-layer process to form nanoscale slippery, lubricant-infused porous coatings (LbL SLIPS). Negative charges are introduced to the substrate (i) and subsequent layers of positively charged polyelectrolyte (ii) and negative charged silica nanoparticles (iii) are adsorbed to form a

hybrid thin film (iv) that can be calcined to produce a porous silica coating (v). After covalently functionalizing the surface with fluorinated silanes (vi), a fluorinated lubricant is wicked into the coating (vii), rendering the surface non-adhesive and allowing for a secondary immiscible liquid to slide off the substrate with ease (viii).

As the process takes advantage of adsorption from aqueous solutions, there is no inherent limit with respect to the area that can be coated. We demonstrate scalability on a laboratory scale by applying the coating process on 17x17 cm^2 glass panels (Figure SI1 and Movie 1). For ease of comparison, we use Krytox™ 100 as fluorinated lubricant for all experiments in this article except the flow experiments, which were performed using the more viscous Krytox™ 103. The choice of lubricants is versatile and, depending on the specific application, lubricants with desired properties can be chosen. For increased long-term stability and applications at elevated temperature, more viscous fluorinated oils with extremely low vapor pressure can be used[30, 39], while oils from natural sources such as olive oil can be selected to ensure non-toxicity.[45]

SEM images of the silica nanoparticle coating on glass substrates prepared with different deposition cycles, taken after calcination at 500°C, are shown in **Figure 2a**. An increase in particle number and film density with increasing deposition cycles is visible. Quartz Crystal Microbalance (QCM) measurements, performed on a silica-coated crystal to ensure similar surface chemistry, further showed evidence of a constant, step-wise addition of silica nanoparticles with each deposition cycle starting after the third cycle (Figure 2b,c and Figure SI 2). This allows for an adjustment of the total roughness and thickness of the coating. The optical properties of the coating after lubrication were investigated by UV-Vis-NIR transmittance measurements. All lubricated substrates showed an increase in light transmittance throughout the visible spectrum compared to a reference glass slide (**Figure 3**). With increasing number of layers, the transmittance of light increased. It has previously been shown that LbL nanoparticle coatings can display superior anti-reflective properties by creating a refractive index gradient along the interface.[15, 53] Here, we simply confirm that the

absence of any hierarchical design allows us to create highly transparent surfaces with liquid repellency properties as we will show below.

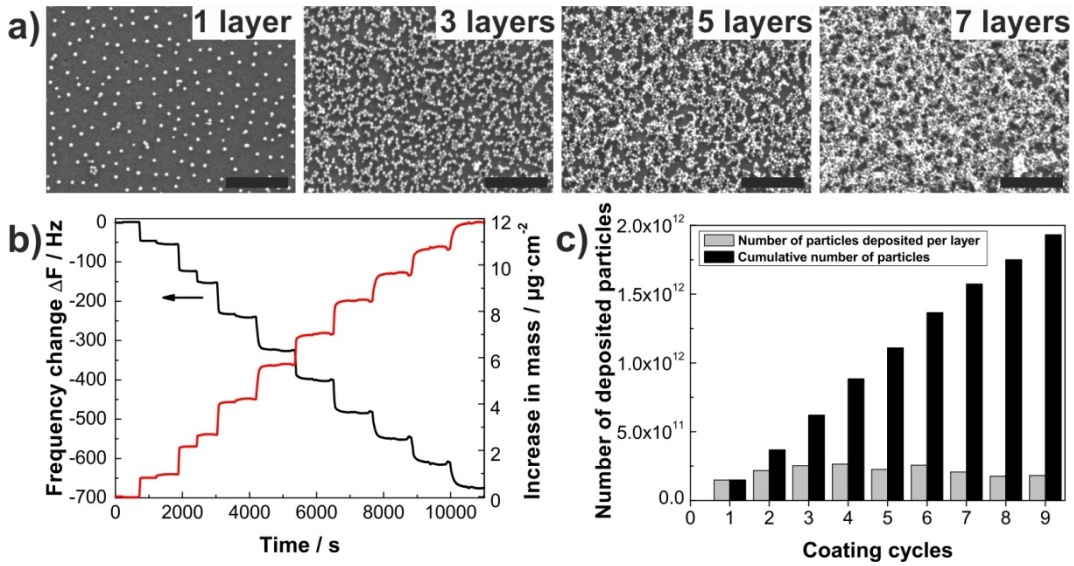

Figure 2. Characterization of the LbL-deposited silica nanoparticle coatings. a) SEM images after different deposition cycles on a glass substrate, taken after calcination to remove the polymer layers. All scale bars are 500 nm. b) Increase in deposited mass for each consecutive LbL adsorption cycle (red line), calculated using Sauerbrey's equation[52] from the frequency drop measured by Quartz Crystal Microbalance (QCM) on a silica-coated crystal (black line). c) Number of silica nanoparticles deposited onto the substrate during each adsorption cycle (gray) and as cumulative during the complete process (black) calculated from the QCM data. A near-linear increase in deposited particles with increasing coating cycles was observed.

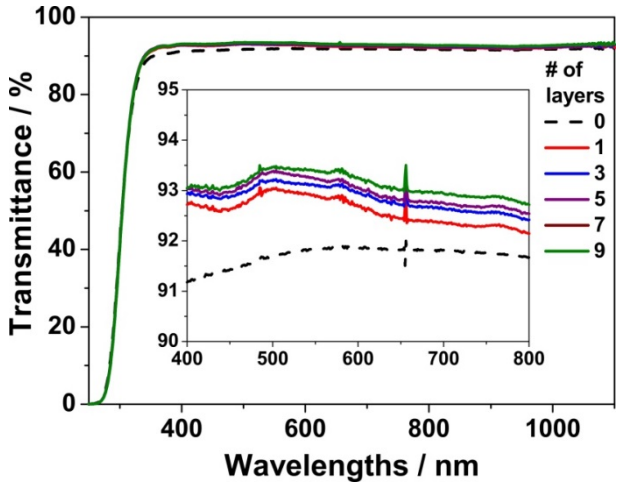

Figure 3. UV-Vis-NIR transmittance spectra of samples lubricated after calcination and fluorosilanization of the silica nanoparticle coating (LbL SLIPS) with increasing numbers of deposited layers show an increase in light transmittance for all coatings as compared to a normal glass slide.

Wetting properties. The wetting properties of the coatings with varying numbers of deposited layers were quantified by dynamic contact angle and sliding angle measurements using water and octane as test liquids on LbL-modified glass slides (**Figure 4**). With increasing coating thickness, the static water contact angle after fluorosilanization steadily increased and leveled at 120° for four or more deposition cycles, indicating complete coverage of the surface with silica nanoparticles (Figure SI3). In contrast to reported silica particle-based coatings,[15-16, 54] the dry coatings do *not* possess superhydrophobic properties due to the small size of the silica nanoparticles and the absence of hierarchical superstructures. As a consequence, a droplet of water placed on a LbL-coated substrate without addition of lubricant experiences significant pinning. This translates to high contact angle hysteresis and removal of a droplet only after tilting the surface to very high angles (Figure 4a,c, light gray columns). Similarly, an octane droplet is pinned and shows significant contact angle hysteresis. Due to its lower surface tension, it starts moving at approximately 35° (Figure 4b,d, light gray columns). However, it leaves a wetted trail behind.

The addition of the lubricant has a significant effect on the wetting properties. If the lubricant is held in place by the surface nanostructures, the added liquid will not be able to penetrate the lubricant layer and will, therefore, experience contact with the fluid lubricant layer only. The molecular smoothness of this liquid/liquid interface eliminates pinning, leading to a minimal contact angle hysteresis and ease of moving of the added droplet without leaving stains on the surface.[30] Figure 4 compares contact angle hysteresis (a,b) and sliding angle measurements (c,d) of water and octane for LbL-coated substrates before and after addition of lubricant as a function of the number of deposited silica nanoparticle layers. For coatings with one or two deposition cycles, the liquid droplets show substantial contact angle hysteresis and high sliding angles, indicating pinning of the liquid at the solid surface.

This result suggests that the ability of the lubricant layer to remain immobilized within the porous network is highly dependent on the number of deposited nanoparticle layers

present on the surface. This behavior correlates well with the SEM and QCM data (Fig. 2) that show uneven, patchy coating structure and non-uniform silica particle accumulation during the first deposition cycles. However, with increasing number of deposited coatings, the surface roughness increases, leading to a more stable solid/lubricant interface as chemical affinity and capillary forces are increased. Coatings with four or more deposited layers showed low contact angle hysteresis and sliding angles for both water and octane, indicating the formation of a stable lubricant layer that is not displaced by the applied liquid. The presence of this stable lubricant layer is demonstrated in Figure 4e,f, which shows the removal of a droplet of water and octane from a lubricated substrate coated with five layers of silica nanoparticles tilted at an angle of 2°. Furthermore, the surfaces retained their repellency properties after application of shear forces induced by spinning at high rotational speeds (Figure SI6,7).

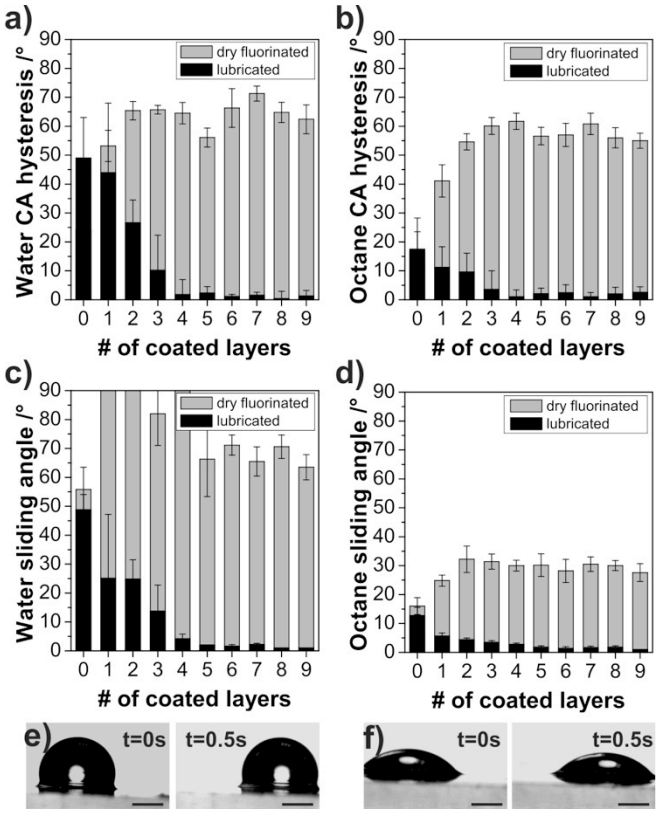

Figure 4: Liquid repellency properties of LbL-silica coatings on glass substrates with and without infiltration with lubricant. a,b) Contact angle (CA) hysteresis of water (a) and octane (b) for LbL silica nanoparticle coatings in dry, fluorosilanized and lubricant-infused state as a function of the number of deposited layers. c,d) Sliding angles of a 20μl droplet of water (c) and octane (d) in dry and lubricated state for coatings with up to nine

deposited layers. The lubricated samples drastically outperform both uncoated (0 layers) and dry coated substrates and feature small contact angle hysteresis and sliding angles for both liquids. All measurements were averaged over 5 individual measurements. e,f) Time-lapse images of a water (e) and octane (f) droplet show sliding under an angle of 2° on a lubricated substrate with five deposited silica nanoparticle layers without getting pinned to the substrate. Scale bars are 1mm.

Coatings on objects with different shapes. The solution-based assembly method also enables the coating to be applied to the interior surfaces of arbitrarily shaped objects. As examples, **Figure 5** shows time-lapsed images taken from Movie 2 and 3 that demonstrate the efficient repellency of honey from the inside of a LbL SLIPS-coated glass vial (Figure 5a, lower row) and of crude oil from the inside of a glass tube (Figure 5b, lower row), visualized by clear sliding of the fluid without adhering to the surface. Honey and crude oil were chosen as examples of challenging sticky and contaminating complex fluids that cannot be removed from uncoated surfaces (Figure 5a,b, upper rows).

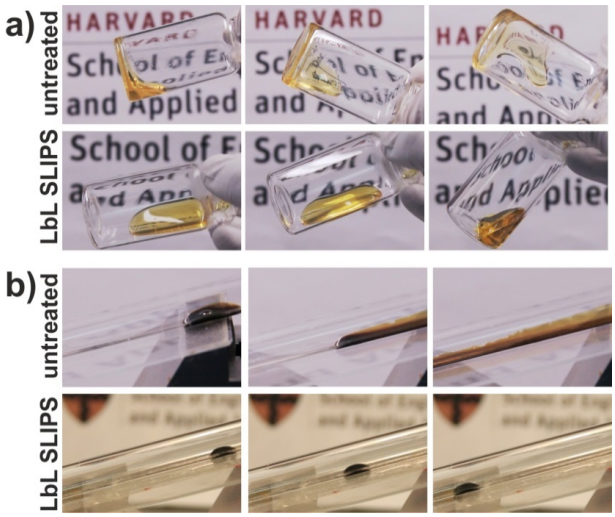

Figure 5. LbL SLIPS coatings repel different complex fluids on arbitrarily-shaped glass surfaces. a) Time-lapsed images taken from Movie 2 showing the sliding of honey in the inside of a glass vial coated with LbL SLIPS (lower row). In contrast, honey strongly sticks to an uncoated glass vial (upper row). b) Time-lapsed images taken from Movie 3 showing the absence of pinning and staining of crude oil in the inside of a LbL SLIPS-coated glass tube (lower row); while an untreated sample is stained by the crude oil (upper row).

Stability of the coating. The repellency performance of lubricant-infused coatings can be compromised in two ways. First, the underlying solid surface topography can be damaged mechanically, leading to de-wetting of the lubricant and the creation of pinning points.[45] Second, lubricant can be drained from or sheared off the surface, exposing solid parts of the surface which then act as pinning points and compromise repellency.[43]

The mechanical properties of the underlying, *solid* nanoparticulate coating were qualitatively examined using a tape peel test. Coatings with nine silica nanoparticle layers were assembled on a silicon wafer substrate and annealed at different temperatures. An adhesive tape (Scotch Magic Tape) was used as a probe to test for the adhesion of the coating to the substrate. 15 repetitions of tape attachment and peel off were performed to guarantee sufficient repetitions to strip off the complete coating. **Figure 6a** shows SEM images of the samples after the peel test. Coatings that were annealed to 500°C were not removed by the adhesive tape, indicating mechanical robustness which can be attributed to an increased sintering of the particles' contact areas.[51] As expected, the wetting properties, measured by water contact angle hysteresis after an additional cleaning step of the substrates to remove traces of adhesive remaining on the substrate showed retained repellency performance on samples with intact nanoparticle coatings (Figure 6b). Samples that were mechanically damaged showed higher contact angle hysteresis, indicative of pinning of the test liquid caused by dewetting of the lubricant.

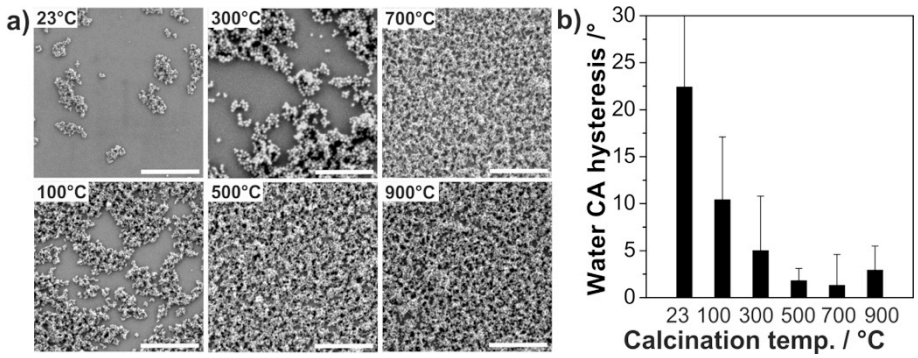

Figure 6. Mechanical properties of the layer-by-layer assembled coatings. Nine layers of a nanoparticle coating were assembled on a silicon wafer substrate, annealed at different temperatures, subjected to a tape peel

test (15 repetitions of peeling with Scotch Magic Tape), imaged by electron microscopy to investigate the damage (a) and infused with a lubricant to test the repellency performance by means of water contact angle hysteresis measurements (b). From a calcination temperature of 500°C, the coatings remained on the substrate without any visible damage and showed retained repellency properties.

To investigate the stability of the *lubricant film*, LbL-coated, lubricant-infused glass tubes were subjected to a continuous flow of water in a closed circulation system. After a set time of water circulation, the flow was stopped, the water was drained and the performance of the coating was evaluated. Sliding angles of individual water droplets (70uL) were measured. **Figure 7a** shows the resulting water sliding angles after continuous water flow at 10 ml/min for up to 5 days. A reference, fluorosilanized sample without a nanoparticulate coating ("coating 0") and a tube coated with a single layer of silica nanoparticles ("coating 1") showed high water sliding angles indicating that the lubricant layer was drained off the substrate, in agreement with the measurements performed on flat surfaces shown in Figure 4. Samples with 5 and 9 nanoparticle layers, showed much lower sliding angles of around 5°, indicative of an intact lubricant layer covering the surface structures.

The flow rate was then increased from 10 ml/min to 100 ml/min and the samples subjected to continuous flow for 24h (Figure 7b). With increased flow rate, the repellency properties of the coating with 5 nanoparticle layers started to become compromised, as can be seen from an increase in sliding angle to 20°. The tube coated with 9 nanoparticle layers retained its low water sliding angles at all tested flow velocities. We therefore conclude that the lubricant layer in LbL coated substrates can be retained even under exposure to long-term flow conditions.

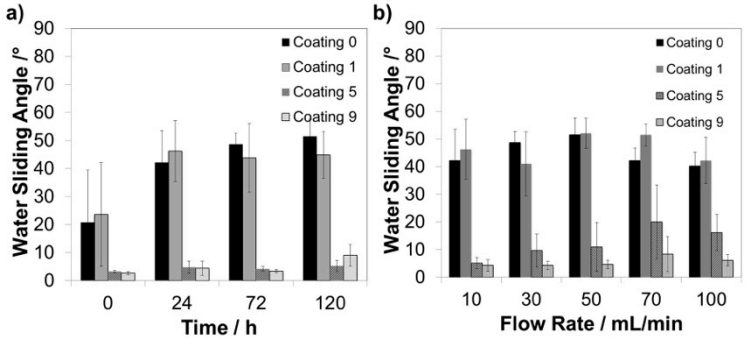

Figure 7. Performance of lubricant-infused LbL coatings under flow. Glass tubes coated with different numbers of nanoparticle layers and infused with a fluorinated lubricant (Krytox 103) were subjected to a continuous flow of water with a flow rate of 10 ml/min for different times (a) and with different flow rates for 24h (b). After the flow was stopped, the water was drained and the sliding angles of individual droplets of water (20μl) recorded to investigate if the coating retained its repellency properties. Coatings with 9 deposited silica nanoparticle layers retained water repellency for all tested times and flow rates.

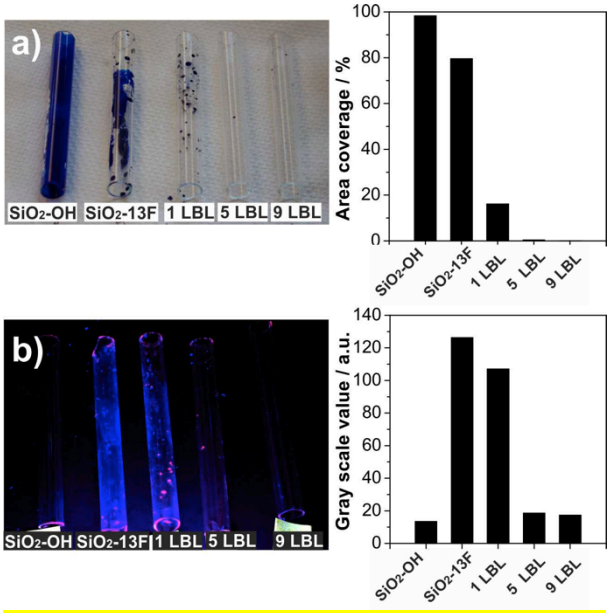

Figure 8. Adhesion and staining of LbL coated, lubricant-infused tubes. Tubes coated with different numbers of nanoparticle layers were subjected to water flow (10 ml/min) for 24 h and then stained with a water-soluble, commercial blue dye (Dharma Pigment 60 Blue Dye) (a) and fluorescently labelled streptavidin proteins (b). Tubes coated with 5 and 9 nanoparticle layers showed negligible staining and a significant decrease in protein adsorption.

Lubricant-infused coatings strongly decrease the adhesion of liquid-borne contaminants.[30, 45] Most crucially, it has been shown that the repellent characteristics extend to biologically relevant materials, including proteins,[45] bacteria[32-33] and marine species.[42] The prevention of adhesion requires an intact lubricant layer to prevent direct contact of the

contaminant with the solid surface. To test for unwanted adhesion, we conditioned samples similar to those described above with water flow (10ml/min) for 24 h and stained the tubes with a commercially available, water-soluble blue dye (Dharma Pigment 60 Blue Dye) and fluorescently labeled streptavidin proteins (incubation time was 10 min) (**Figure 8**). Quantitative information was extracted by image analysis (Figure SI4, Table SI1, Figure SI5, Table SI3). Figure 8a shows that both the hydrophilic glass control, the fluorosilanized glass control without any silica nanoparticles ("SiO_2-13F") and, to a lesser extent, the sample with one deposited silica nanoparticle cycle were stained by the dye, while the samples coated with more silica nanoparticles (5 and 9 layers) showed no visible adhered dye. The adsorption of proteins was visible under UV-light illumination (Figure 8b) and showed strong adsorption on fluorosilanized samples with no or one LbL layer. Since proteins are known to adhere well to hydrophobic surfaces,[3] we attribute the observed protein adhesion to a loss of the liquid lubricant overlayer. Samples with 5 and 9 nanoparticle layers showed little protein adsorption.

Application on different materials. The LbL deposition process can be applied to various substrate materials given that two requirements are met: First, charges need to be introduced to the material's surface to enable the deposition process. This can be achieved by a variety of methods, including treating the substrates with oxygen plasma, UV-ozone, acid or base piranha or a corona discharger. While base piranha provided a simple method to coat both interior and exterior surfaces on glass with LbL-deposited nanoparticulate films, we found that oxygen plasma treatment for short times (1 min, 10sccm gas flow, 100W) was most effective to coat different substrate materials, including metal and polymer surfaces. Second, after successful deposition, the surfaces of the silica nanoparticle coating need to be oxidized to create hydroxyl functional groups necessary to covalently bind the fluorinated silane molecules that are thereby required to match the surface chemistry of the lubricant. For glass surfaces, calcination at elevated temperatures was used to completely remove the organic

polycation layer prior to a base piranha-mediated surface activation. For different substrate materials, especially polymer substrates, calcination is not possible. We therefore revised the process and used oxygen plasma to combust the polycation surface layers and oxidize the silica nanoparticle surfaces. This revised process limits the applicability to surfaces that can be efficiently treated with plasma. Shielded or highly curved substrates, for example the inside of a tube cannot be efficiently coated using this process. We compared the stability of the lubricant layer under shear forces for both methods and found no differences in lubricant layer thicknesses and repellency performance between calcined and oxygen plasma-treated samples (Figure SI6, 7).

As examples of the LbL SLIPS formation on metal or polymer surfaces, we investigated the coating process on aluminum and poly(methylmethacrylate) (PMMA) substrates, respectively. The consecutive build-up of nanoparticle layers on aluminum was visible in SEM images (Figure SI8), while the increase in static water contact angles with increasing number of nanoparticle layers (Figure SI9) indicates a successful functionalization with (1H,1H,2H,2H-tetrahydrotridecafluorooctyl)-trichlorosilane. The wetting properties of the LbL-coated aluminum and PMMA films were investigated before and after infusion of lubricant by means of contact angle hysteresis measurements using octane as a test liquid (**Figure 9**a,c).

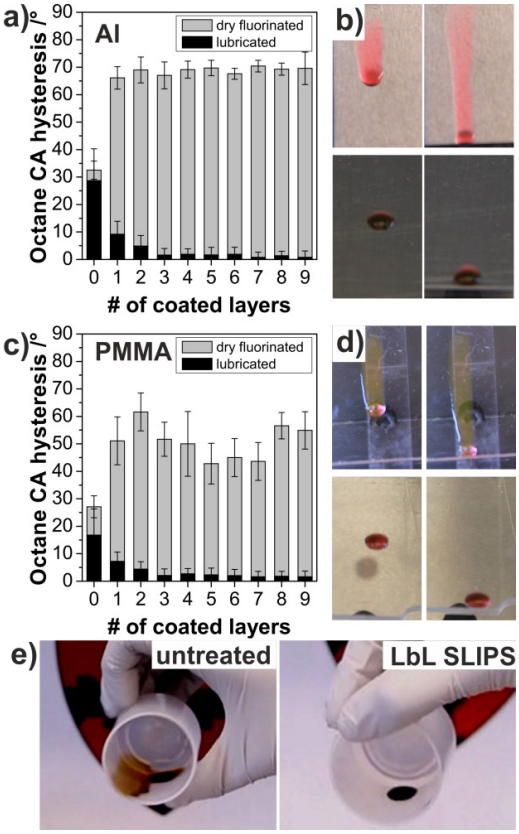

Figure 9. LbL SLIPS coatings on different materials. a) Contact angle hysteresis of octane as a function of the number of LbL cycles on an aluminum substrate with and without addition of lubricant. b) Wetting properties of a dyed octane droplet moving along a surface of untreated (top row) and LbL SLIPS-coated aluminum with five deposited silica nanoparticle layers (lower row) under a tilt angle of 20°. In contrast to the untreated sample, no staining is observed for the coated surface. c) Contact angle hysteresis of octane as a function of the number of LbL cycles on a PMMA substrate with and without addition of lubricant. d) Wetting properties of an uncoated and LbL SLIPS-modified PMMA surface with five deposited silica nanoparticle layers. Similar to glass and aluminum surfaces, a dyed octane droplet leaves no stains on the coated polymer surface. The tilt angle was 20°. e) Example of a LbL SLIPS coating on curved polymer surfaces: The images show the absence of staining of crude oil in a LbL SLIPS-coated polypropylene jar.

Similar to the coatings on glass substrates, LbL-SLIPS on aluminum and PMMA substrates showed a significantly lower contact angle hysteresis than dry, fluorosilanized coatings. Substrates coated with three or more layers showed octane contact angle hysteresis well below 5°, indicating a stable lubricant layer covering the substrate. In contrast to untreated and dry, fluorosilanized coatings, an octane droplet moving along the SLIPS substrates did not leave any residue on either aluminum or PMMA surfaces (Figure 9b,d, Figure SI10a). The coating process can also be applied to curved surfaces as long as the surface is accessible to

oxygen plasma. As a proof-of-principle, we show the application of repellent coatings on an Eppendorf tube and a polypropylene jar (Movie 4,5, Figure 9e).

Table 1. Sliding angles averaged over five individual measurements, of octane and water droplets on different substrates coated with LbL silica nanoparticles (seven deposited layers).

Substrate	**Water sliding angle /°**			**Octane sliding angle /°**		
Material	Untreated	Dry coating	Lubricated coating	Untreated	Dry coating*	Lubricated coating**
Glass	56±8	66±5	2.2±0.5	16±3	31±3	1.6±0.5
Aluminum	pinned	63±4	2.2±0.4	wetted	51±13	2.0±0.7
Stainless Steel	pinned	85±5	1.4±0.5	wetted	49±7	1.4±0.5
PMMA	pinned	pinned	2.0±0.7	wetted	46±5	1.6±0.5
Poly propylene	pinned	pinned	1.2±0.4	wetted	48±6	1.4±0.7
Poly sulfone	pinned	pinned	2.4±0.5	wetted	44±5	2.0±0.7

*octane droplet left stains on the surface after sliding
**no contamination of the surface after sliding

Further examples of successfully coated surfaces include stainless steel, poly propylene (PP) and polysulfone (PSu) (Figure SI10b). **Table 1** quantifies the wetting behavior of all tested substrates by comparing the sliding angles of water and octane for untreated reference samples; dry, fluorosilanized layer-by-layer silica nanoparticle coatings (7 deposition cycles), and the same coatings after addition of lubricant (dynamic contact angles and contact angle hysteresis data are shown in Table SI5 and Table SI6). All untreated reference samples failed to repel water as the droplets remained pinned even after tilting the substrate to 90°, and were wetted and stained by octane. The introduction of the dry, fluorosilanized LbL surface coating changed the wetting properties consistently for all samples and showed high contact angle hysteresis and sliding angles for both liquids. The presence of octane stains on the surfaces indicated the failure of the dry coating in repelling the liquid. All functionalized, lubricated samples showed small sliding angles and absence of staining for both water and octane.

3. Conclusions

We have developed a simple process to introduce a lubricant-infused, repellent coating to a variety of surface materials and shapes. The surface structure consists of a nanoscale colloidal film prepared by a cycled adsorption of positively charged polyelectrolytes and negatively charged silica nanoparticles. After fluorosilanization of the silica nanoparticles, a fluorinated lubricant is infiltrated into the porous coating and firmly held in place by matching surface chemistry and surface roughness. The strong affinity of the lubricant to the substrate ensures the stability of the lubricating film and creates a barrier that prevents a second liquid from being exposed to the underlying solid. With the absence of pinning points, the applied liquids slide off the substrate with ease.

We performed a detailed analysis of the structural, wetting, optical and mechanical properties of such LbL SLIPS and demonstrated the range of their functional advantages: (1) with the increasing number of deposited silica nanoparticle layers, the coating demonstrates successful repellency of aqueous, organic and complex liquids, including biological fluids; (2) it can be formed on arbitrarily shaped glass surfaces; (3) the coating protocol can be modified to apply to different material classes, including metal and polymeric surfaces; (4) the small size of the silica nanoparticles applied in the process does not interfere with light of visible wavelengths and, thus, gives rise to transparency of the coating, a prerequisite for potential application in self-cleaning, stain-resistant windows, solar panels or lenses; (5) the coatings retained their repellent properties after exposure to flow; (6) upon annealing at high temperatures, the coating produces a mechanically robust layer due to the sintering of silica particles; (7) the deposition process is simple, of low cost, based on aqueous solutions and thus environmentally benign, scalable and automatable. The presented method thus combines all the remarkable properties of previously reported lubricant-infused coatings with improved simplicity and versatility of accessible substrate materials, shapes and sizes. We expect this

process to be commensurate with industrial coating procedures and to have impact in the general design of highly repellent, self-cleaning, non-fouling, transparent surfaces.

4. Experimental Section

Materials. Sulfuric acid, hydrogen peroxide (33% in water), ammonia (25% in water), poly(diallyldimethylammonium) chloride (20% in water), Ludox TM40 silica nanoparticles (diameter: 20nm), (1H,1H,2H,2H-tetrahydrotridecafluorooctyl)-trichlorosilane (13F), poly methyl methacrylate and Toluene were purchased from Sigma Aldrich and used without further purification. MilliQ (Millipore, Billerica, MA, USA) water was used for all experiments. Flat 5 cm x 3 cm x 0.1 cm Aluminum, Stainless steel and polymer substrates were purchased from McMaster. Borosilicate glass pipettes (VWR) were cut in 10 cm lengths as substrates used in all flow experiments. The DuPont Krytox PFPE GPL 100 lubricant was purchased from Miller-Stephenson (Density 1870 kg/m^3 at 0°C; kinematic viscosity 0.12 cm^2/s, evaporation rate 0.59%/day[30]). Mustard and honey were purchased from Market Basket. The crude oil used was a naphthenic crude oil (Hoops) from Texas, USA (North America) with a medium-heavy density of 0.869 g/ml (31.4*API) at 15.56°C and 1.00% sulfur (sour with more than 0.50% sulfur) and a TAN of 0.92 mg KOH/g. Optical transmission of glass substrates and their SLIPS-coated counterparts were measured at room temperature using an Agilent 8453 UV-Vis spectrometer with air as the background. All SEM images were taken using a Zeiss FESEM Ultra Plus.

Deposition of Colloidal Particles onto Substrates. Glass substrates were immersed into base piranha (5:1:1 water to hydrogen peroxide solution to ammonia solution) at 80 °C for 0.5 h to remove any organic residues. All metal and polymer substrates were oxygen plasma treated for 1 min to create surface charges. After this cleaning treatment, the substrates were rinsed in DI water. The layer-by-layer deposition was performed by immersion of the substrates in a

0.1 wt.-% solution of poly(diallyldimethylammonium) chloride (PDADMAC) for 10 min, followed by rinsing in DI water for 1 min and subsequent immersion into a solution of 0.1 wt.-% Ludox silica colloids for 10 min and rinsing for 1 min in water. This cycle was repeated to deposit multilayers.

Removal of Polymer Layer. The organic material was removed by combustion at 500 °C (ramped from room temperature to 500 °C for 5 h, 2 h at 500°C, ramped from 500°C back to room temperature in 2 h) in the case of glass substrates. All other samples were treated with oxygen plasma (Model femto, Plasma Diener, Germany) for 1min with 10sccm oxygen gas flow and 100W power to partially degrade the polyelectrolyte and activate the silica surface.

Fluorosilanization. Fluorosilanization was carried out by vapor-phase deposition of (1H,1H,2H,2H-tetrahydrotridecafluorooctyl)-trichlorosilane for 24 h at reduced pressure and room temperature. Prior to silanization, the substrates were cleaned in base piranha (glass substrates) or plasma-treated with oxygen plasma as described above for metal or polymer substrates.

Lubrication. 10µl/cm^2 substrate of DuPont Krytox 100 was added to the substrate until uniform coverage was achieved by tilting. To achieve a homogeneous lubricant layer thickness for all different samples and experiments and thus allow proper comparison, all samples were placed vertically for 10 min in order to thin out the lubricant film by gravity-assisted drainage.

Quartz Crystal Microbalance Measurements. Measurements were performed on an E4 Auto QCM-D from Q-sense (Sweden) using silica-coated quartz crystal. Prior to the layer-by-layer deposition and data collection, the crystal was cleaned of organic residue using base piranha (5:1:1 water to hydrogen peroxide solution to ammonia solution) for 1 min at 75 °C and then UV-Ozone treated for 10 min. Each layer deposition was performed for 7 min at 100 uL/min flow of alternating PDADMA and 20 nm silica colloid solution with a 2 min H_2O rinse in

between each deposition at 300 uL/min. The concentration of both solutions was similar to bulk deposition experiments (0.1 wt. %)

Contact angle measurements. Dynamic contact angles were measured using a goniometer (CAM 101, KSV Instruments) at ambient condition by slowly increasing and decreasing the volume of the droplet to induce sliding, then analyzing the images to find the best fitting contact angles. All measurements were repeated at least five times on different areas of the substrates and averaged. Sliding angles were determined using a 10µl droplet of liquid on a customized tilting stage with a precision of approximately 0.5°. All measurements were averaged over at least five droplets. To be counted as "sliding", a droplet needed to slide over the full substrate without getting pinned at any point.

Flow experiments. All flow experiments were conducted using the Masterflex L/S Peristaltic Pump (Cole-Parmer). The glass tubes coated with the desired layer number were infused with 200 µL of DuPont Krytox 103 and left vertically tilted for 10 min to drain excess lubricant. They were subsequently connected to silicone tubing and conditioned with water for 20 min at 10 ml/min with water flowing out of the glass tubes and collecting in a waste container. After the conditioning step, a closed loop of the silicone tube and the glass tube was created before beginning water circulation. Care was taken to avoid air bubbles. After specific time points at the desired flow rate, the flow was stopped and the water drained from the tube. Then, sliding angles were measured using individual 70 µL droplets of water on a tilting stage. All measurements were averaged over at least five droplets. All experiments were performed in triplicate. For the staining experiments, a water soluble blue dye (Dharma Pigment 60 Blue Dye, Dharma Trading Co.) was mixed with water in a 1:4 ratio. The glass tube samples subjected to 24 h of water flow at 10 ml/min were held at an approximately 45° tilt while 1 mL of the prepared solution was added drop wise into each tube and rotated to ensure exposure to the entire surface of the tube. Then, the tube was tilted vertically to drain

excess dye solution. Data quantification was performed with ImageJ as specified in the supporting information.

Protein adhesion. After 24 h of DI water flow at 10 ml/min, 1 mL of Alexa Fluor 350 conjugated streptavidin (Life Technologies) solution at a concentration of 0.06 mg/ml was flowed in the glass tubes for 10 min. The samples were subsequently illuminated with UV light at an excitation wavelength of 350 nm to indicate areas of protein adhesion to the tube surface. Images were taken upon UV excitation and further quantified using ImageJ as specified in the supporting information.

Tape peel test. 9 bilayers of PDADMA and silica spheres were assembled onto a silicon wafer as described above. The samples were sintered at 100 °C, 300 °C, 500 °C, 700 °C, and 1100 °C (ramped at 2°C/min from room temperature to the specified temperature, 2 h at the specified temperature, and then ramped down at 2°C/min to room temperature). Adhesive tape (Scotch Magic Tape) was applied and removed from the samples fifteen times and then imaged using scanning electron microscopy to determine the degree of silica removal from the substrate. Before imaging in the SEM, the samples were subjected to piranha to remove adhesive residues on the substrate.

Supporting Information
Additional movies, experimental details, lubricant film thickness and stability under shear, LbL coatings on different materials are shown in Supporting Information.
Supporting Information is available from the Wiley Online Library or from the author.

Acknowledgements
N.V. acknowledges support from the Leopoldina Fellowship Programme. S.S. acknowledges support from the Natural Sciences and Engineering Research Council of Canada. The work was supported by the ARPA-E under award number DE-AR0000326 (fabrication and surface properties) and by the AFOSR under award number FA9550-09-0669-DOD35CAP (optical properties). This work was performed in part at the Harvard Center for Nanoscale Systems (CNS) supported by the NSF under award number ECS-0335765. S.S. and N.V. contribute equally to the research presented in this manuscript.

Received: ((will be filled in by the editorial staff))
Revised: ((will be filled in by the editorial staff))
Published online: ((will be filled in by the editorial staff))

References

[1] A. Tuteja, W. Choi, M. L. Ma, J. M. Mabry, S. A. Mazzella, G. C. Rutledge, G. H. McKinley, R. E. Cohen, *Designing superoleophobic surfaces, Science* **2007**, *318*, 1618-1622.

[2] A. Tuteja, W. Choi, J. M. Mabry, G. H. McKinley, R. E. Cohen, *Robust omniphobic surfaces, Proc. Natl. Acad. Sci. U. S. A.* **2008**, *105*, 18200-18205.

[3] G. B. Sigal, M. Mrksich, G. M. Whitesides, *Effect of surface wettability on the adsorption of proteins and detergents, Journal of the American Chemical Society* **1998**, *120*, 3464-3473.

[4] R. O. Darouiche, *Device-associated infections: A macroproblem that starts with microadherence, Clinical Infectious Diseases* **2001**, *33*, 1567-1572.

[5] R. S. Friedlander, H. Vlamakis, P. Kim, M. Khan, R. Kolter, J. Aizenberg, *Bacterial flagella explore microscale hummocks and hollows to increase adhesion, Proc. Natl. Acad. Sci. U. S. A.* **2013**, *110*, 5624-5629.

[6] W. Barthlott, C. Neinhuis, *Purity of the sacred lotus, or escape from contamination in biological surfaces, Planta* **1997**, *202*, 1-8.

[7] L. Feng, S. H. Li, Y. S. Li, H. J. Li, L. J. Zhang, J. Zhai, Y. L. Song, B. Q. Liu, L. Jiang, D. B. Zhu, *Super-hydrophobic surfaces: From natural to artificial, Adv. Mater.* **2002**, *14*, 1857-1860.

[8] D. Quere, *Non-sticking drops, Rep. Prog. Phys.* **2005**, *68*, 2495-2532.

[9] X. J. Feng, L. Jiang, *Design and creation of superwetting/antiwetting surfaces, Adv. Mater.* **2006**, *18*, 3063-3078.

[10] B. Bhushan, Y. C. Jung, *Natural and biomimetic artificial surfaces for superhydrophobicity, self-cleaning, low adhesion, and drag reduction, Progress in Materials Science* **2011**, *56*, 1-108.

[11] X. Deng, L. Mammen, H. J. Butt, D. Vollmer, *Candle soot as a template for a transparent robust superamphiphobic coating, Science* **2012**, *335*, 67-70.

[12] R. Poetes, K. Holtzmann, K. Franze, U. Steiner, *Metastable underwater superhydrophobicity, Phys. Rev. Lett.* **2010**, *105*.

[13] H. Mertaniemi, V. Jokinen, L. Sainiemi, S. Franssila, A. Marmur, O. Ikkala, R. H. A. Ras, *Superhydrophobic tracks for low-friction, guided transport of water droplets, Adv. Mater.* **2011**, *23*, 2911-2914.

[14] J. V. I. Timonen, M. Latikka, L. Leibler, R. H. A. Ras, O. Ikkala, *Switchable static and dynamic self-assembly of magnetic droplets on superhydrophobic surfaces, Science* **2013**, *341*, 253-257.

[15] J. Bravo, L. Zhai, Z. Wu, R. E. Cohen, M. F. Rubner, *Transparent superhydrophobic films based on silica nanoparticles, Langmuir* **2007**, *23*, 7293-7298.

[16] L. Zhai, F. Ç. Cebeci, R. E. Cohen, M. F. Rubner, *Stable superhydrophobic coatings from polyelectrolyte multilayers, Nano Lett.* **2004**, *4*, 1349-1353.

[17] D. Lee, M. F. Rubner, R. E. Cohen, *All-nanoparticle thin-film coatings, Nano Lett.* **2006**, *6*, 2305-2312.

[18] G. Decher, *Fuzzy nanoassemblies: Toward layered polymeric multicomposites, Science* **1997**, *277*, 1232-1237.

[19] G. Decher, J. D. Hong, J. Schmitt, *Buildup of ultrathin multilayer films by a self-assembly process .3. Consecutively alternating adsorption of anionic and cationic polyelectrolytes on charged surfaces, Thin Solid Films* **1992**, *210*, 831-835.

[20] F. Caruso, *Nanoengineering of particle surfaces, Adv. Mater.* **2001**, *13*, 11

[21] P. T. Hammond, *Form and function in multilayer assembly: New applications at the nanoscale, Adv. Mater.* **2004**, *16*, 1271-1293.
[22] Z. Y. Tang, Y. Wang, P. Podsiadlo, N. A. Kotov, *Biomedical applications of layer-by-layer assembly: From biomimetics to tissue engineering, Adv. Mater.* **2006**, *18*, 3203-3224.
[23] K. Ariga, J. P. Hill, Q. M. Ji, *Layer-by-layer assembly as a versatile bottom-up nanofabrication technique for exploratory research and realistic application, Phys. Chem. Chem. Phys.* **2007**, *9*, 2319-2340.
[24] A. Javey, S. Nam, R. S. Friedman, H. Yan, C. M. Lieber, *Layer-by-layer assembly of nanowires for three-dimensional, multifunctional electronics, Nano Lett.* **2007**, *7*, 773-777.
[25] Y. Wang, A. S. Angelatos, F. Caruso, *Template synthesis of nanostructured materials via layer-by-layer assembly, Chemistry of Materials* **2008**, *20*, 848-858.
[26] P. T. Hammond, *Building biomedical materials layer-by-layer, Mater. Today* **2012**, *15*, 196-206.
[27] S. W. Morton, Z. Y. Poon, P. T. Hammond, *The architecture and biological performance of drug-loaded lbl nanoparticles, Biomaterials* **2013**, *34*, 5328-5335.
[28] K. Saetia, J. M. Schnorr, M. M. Mannarino, S. Y. Kim, G. C. Rutledge, T. M. Swager, P. T. Hammond, *Spray-layer-by-layer carbon nanotube/electrospun fiber electrodes for flexible chemiresistive sensor applications, Adv. Funct. Mater.* **2014**, *24*, 492-502.
[29] A. Lafuma, D. Quere, *Slippery pre-suffused surfaces, European Physics Journal* **2011**, *96*, 56001.
[30] T. S. Wong, S. H. Kang, S. K. Y. Tang, E. J. Smythe, B. D. Hatton, A. Grinthal, J. Aizenberg, *Bioinspired self-repairing slippery surfaces with pressure-stable omniphobicity, Nature* **2011**, *477*, 443-447.
[31] J. D. Smith, R. Dhiman, S. Anand, E. Reza-Garduno, R. E. Cohen, G. H. McKinley, K. K. Varanasi, *Droplet mobility on lubricant-impregnated surfaces, Soft Matter* **2013**, *9*, 1772-1780.
[32] A. K. Epstein, T. S. Wong, R. A. Belisle, E. M. Boggs, J. Aizenberg, *Liquid-infused structured surfaces with exceptional anti-biofouling performance, Proc. Natl. Acad. Sci. U. S. A.* **2012**, *109*, 13182-13187.
[33] J. Li, T. Kleintschek, A. Rieder, Y. Cheng, T. Baumbach, U. Obst, T. Schwartz, P. A. Levkin, *Hydrophobic liquid-infused porous polymer surfaces for antibacterial applications, ACS Appl. Mater. Interfaces* **2013**, *5*, 6704-6711.
[34] P. Kim, T.-S. Wong, J. Alvarenga, M. J. Kreder, W. E. Adorno-Martinez, J. Aizenberg, *Liquid-infused nanostructured surfaces with extreme anti-ice and anti-frost performance, ACS Nano* **2012**, *6*, 6569-6577.
[35] K. Rykaczewski, S. Anand, S. B. Subramanyam, K. K. Varanasi, *Mechanism of frost formation on lubricant-impregnated surfaces, Langmuir* **2013**, *29*, 5230-5238.
[36] J. Chen, R. Dou, D. Cui, Q. Zhang, Y. Zhang, F. Xu, X. Zhou, J. Wang, Y. Song, L. Jiang, *Robust prototypical anti-icing coatings with a self-lubricating liquid water layer between ice and substrate, ACS Appl. Mater. Interfaces* **2013**, *5*, 4026-4030.
[37] X. Yao, Y. Hu, A. Grinthal, T.-S. Wong, L. Mahadevan, J. Aizenberg, *Adaptive fluid-infused porous films with tunable transparency and wettability, Nat Mater* **2013**, *12*, 529-534.
[38] T. S. Wong, T. H. Chen, X. Shen, C. M. Ho, *Nanochromatography driven by the coffee ring effect, Analytical Chemistry* **2011**, *83*, 1871-1873.
[39] D. Daniel, M. N. Mankin, R. A. Belisle, T.-S. Wong, J. Aizenberg, *Lubricant-infused micro/nano-structured surfaces with tunable dynamic omniphobicity at high temperatures, Applied Physics Letters* **2013**, *102*, -.

[40] S. Anand, A. T. Paxson, R. Dhiman, J. D. Smith, K. K. Varanasi, *Enhanced condensation on lubricant-impregnated nanotextured surfaces, ACS nano* **2012**, *6*, 10122-10129.

[41] R. Xiao, N. Miljkovic, R. Enright, E. N. Wang, *Immersion condensation on oil-infused heterogeneous surfaces for enhanced heat transfer, Sci. Rep.* **2013**, *3*.

[42] L. L. Xiao, J. S. Li, S. Mieszkin, A. Di Fino, A. S. Clare, M. E. Callow, J. A. Callow, M. Grunze, A. Rosenhahn, P. A. Levkin, *Slippery liquid-infused porous surfaces showing marine antibiofouling properties, ACS Appl. Mater. Interfaces* **2013**, *5*, 10074-10080.

[43] P. Kim, M. J. Kreder, J. Alvarenga, J. Aizenberg, *Hierarchical or not? Effect of the length scale and hierarchy of the surface roughness on omniphobicity of lubricant-infused substrates, Nano Lett.* **2013**, *13*, 1793-1799.

[44] W. Ma, Y. Higaki, H. Otsuka, A. Takahara, *Perfluoropolyether-infused nano-texture: A versatile approach to omniphobic coatings with low hysteresis and high transparency, Chem. Commun.* **2013**, *49*, 597-599.

[45] N. Vogel, R. A. Belisle, B. Hatton, T.-S. Wong, J. Aizenberg, *Transparency and damage tolerance of patternable omniphobic lubricated surfaces based on inverse colloidal monolayers, Nat Commun* **2013**, *4, 2167*.

[46] R. N. Wenzel, *Resistance of solid surfaces to wetting by water, Industrial and Engineering Chemistry* **1936**, *28*, 988-994.

[47] A. B. D. Cassie, S. Baxter, *Wettability of porous surfaces, Trans. Faraday Soc.* **1944**, *40*, 0546-0550.

[48] X. Huang, J. D. Chrisman, N. S. Zacharia, *Omniphobic slippery coatings based on lubricant-infused porous polyelectrolyte multilayers, ACS Macro Letters* **2013**, 826-829.

[49] S. S. Qureshi, Z. Q. Zheng, M. I. Sarwar, O. Felix, G. Decher, *Nanoprotective layer-by-layer coatings with epoxy components for enhancing abrasion resistance: Toward robust multimaterial nanoscale films, ACS nano* **2013**, *7*, 9336-9344.

[50] K. Ariga, Y. Lvov, M. Onda, I. Ichinose, T. Kunitake, *Alternately assembled ultrathin film of silica nanoparticles and linear polycations, Chem. Lett.* **1997**, 125-126.

[51] Z. Gemici, H. Shimomura, R. E. Cohen, M. F. Rubner, *Hydrothermal treatment of nanoparticle thin films for enhanced mechanical durability, Langmuir* **2008**, *24*, 2168-2177.

[52] G. Sauerbrey, *Verwendung von schwingquarzen zur wagung dunner schichten und zur mikrowagung, Zeitschrift Fur Physik* **1959**, *155*, 206-222.

[53] H. Shimomura, Z. Gemici, R. E. Cohen, M. F. Rubner, *Layer-by-layer-assembled high-performance broadband antireflection coatings, ACS Appl. Mater. Interfaces* **2010**, *2*, 813-820.

[54] H.-J. Tsai, Y.-L. Lee, *Facile method to fabricate raspberry-like particulate films for superhydrophobic surfaces, Langmuir* **2007**, *23*, 12687-12692.

[55] O. Gavet, J. Pines, *(2010) Progressive activation of CyclinB1-Cdk1 coordinates entry to mitosis. Dev Cell,* **2010,** 18, 533-543.

Table of contents entry

Lubricant-infused coatings provide efficient repellency of various liquids and prevent the adhesion of liquid-borne contaminants. Here, a simple layer-by-layer deposition process is used to create functional, transparent, mechanically robust and stable lubricant-infused coatings on a variety of different materials with arbitrary shapes.

Keyword Functional Coatings

Steffi Sunny, Nicolas Vogel, Caitlin Howell, Thy L. Vu, and Joanna Aizenberg**

Title Lubricant-infused Nanoparticulate Coatings Assembled by Layer-by-layer Deposition

ToC figure

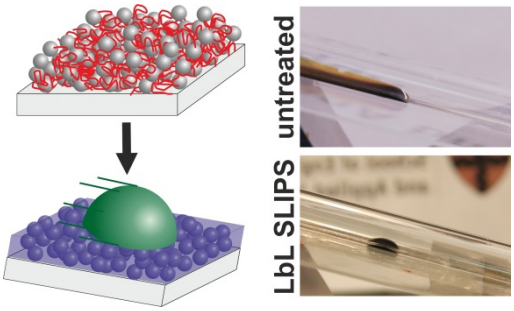

Supporting Information

Lubricant-infused Nanoparticulate Coatings Assembled by Layer-by-layer Deposition

Steffi Sunny,[1,§] Nicolas Vogel,[1,§,] Caitlin Howell,[2] Thy L. Vu,[2] and Joanna Aizenberg[1,2,3,*]*
[1]School of Engineering and Applied Sciences, Harvard University, Cambridge, MA 02138, USA
[2]Wyss Institute for Biologically Inspired Engineering, Harvard University, Cambridge, MA 02138, USA
[3]Department of Chemistry and Chemical Biology, Harvard University, Cambridge, MA 02138, USA

Contents:

Available movies:

Movie 1: Larger size glass panels coated with layer-by-layer SLIPS repel water and olive oil
Movie 2: Honey moves in a vial without getting pinned
Movie 3: Crude oil slides through a glass tube
Movie 4: LbL SLIPS coatings on curved plastic surfaces repel dyed water
Movie 5: LbL SLIPS coatings on curved plastic surfaces repel crude oil

1) Large area substrates

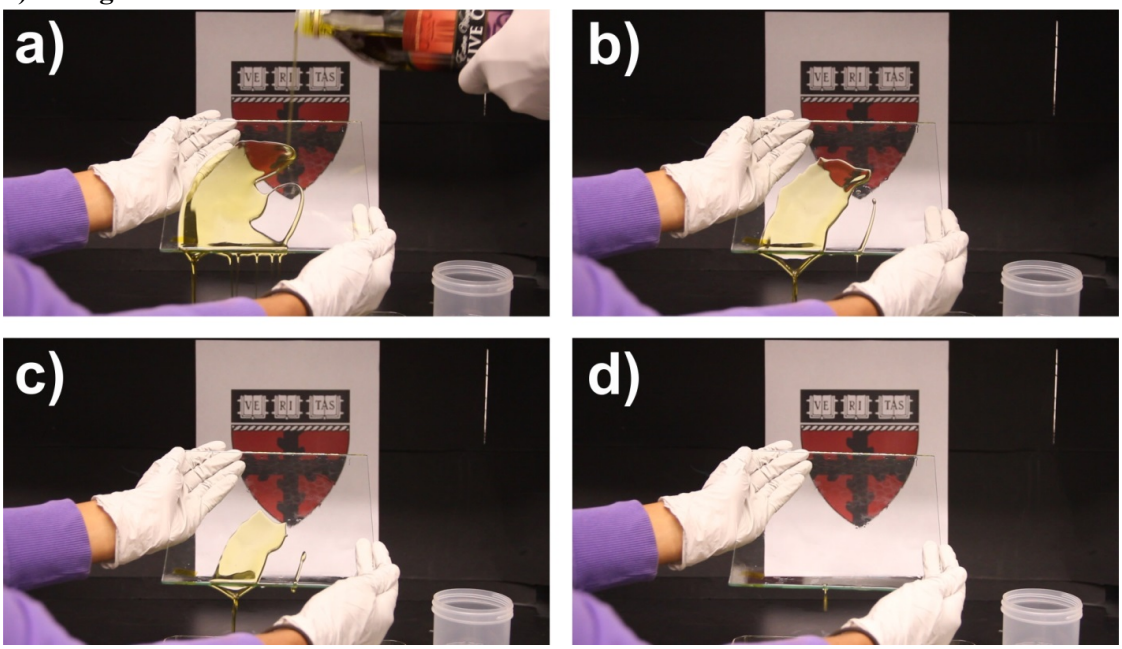

Figure SI1. A LbL SLIPS coating (5 deposited layers) on a large, 17x17 cm^2 glass panel demonstrating scalability of the process. The pictures are time-lapsed images showing the repellency of olive oil from the coated glass panel and are taken from Movie 1.

2) Quartz Crystal Microbalance data

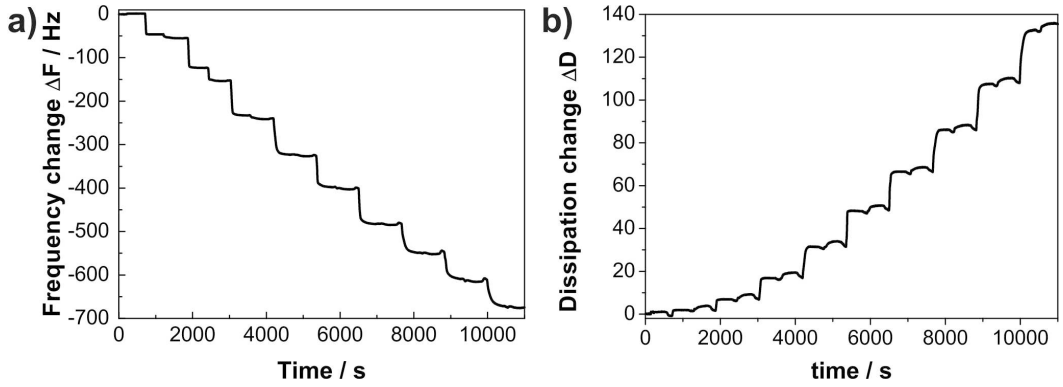

Figure SI2: QCM-D data: change in resonance frequency (a) and dissipation (b). As the dissipation is much smaller than the change in resonance frequency, the system can be treated as a stiff film and the resonance frequency change can be directly converted into the deposited mass using Sauerbrey's equation.[41]

3) Contact angles of water on dry, fluorosilanized samples

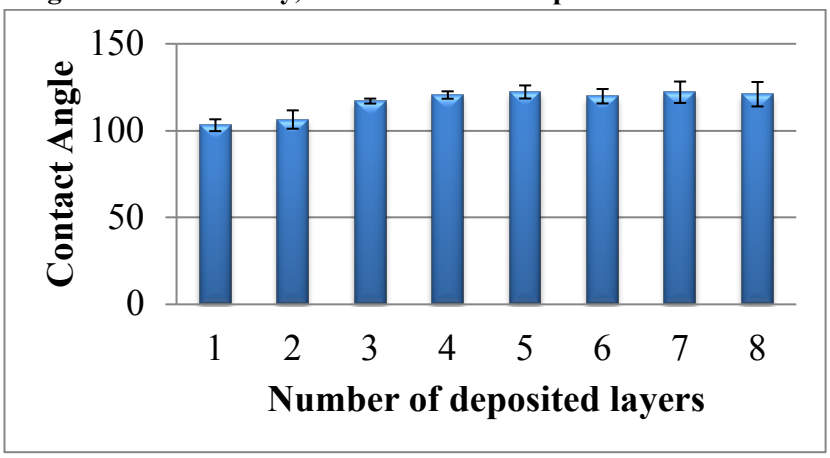

Figure SI3: Static contact angles of dry, fluorosilanized coatings with different layer thicknesses. The water contact angle levels at 120° for coating with four layers onwards, indicating a complete filling of the substrate with particles. The surfaces do not show superhydrophobic properties due to the small size of the nanoparticles (diameter 20nm).

4) Quantification of adhesion data

The center cross-section from each of the glass tubes in the Figure 8a image was cut in equal dimensions as a representative portion of the entire tube. The images were processed using the ImageJ threshold feature to generate corresponding images with black areas representing coverage by the blue dye (Figure SI4). The software was subsequently used to determine the area covered by the black regions (Table SI1).

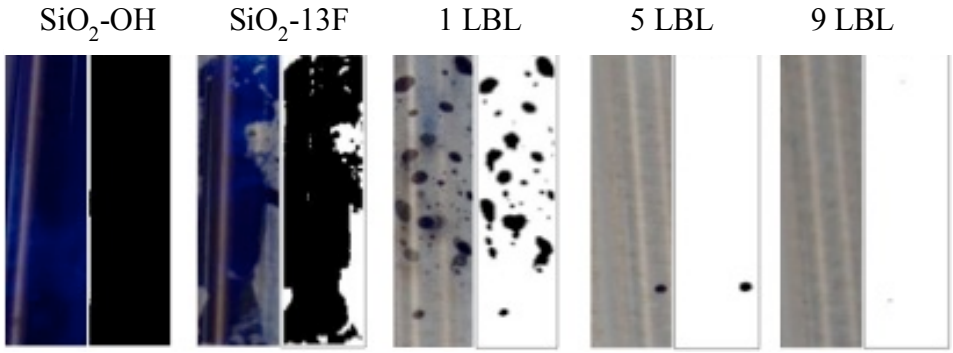

Figure SI4. Glass tubes treated with Dharma Pigment 60 Blue Dye (after 24 hours of water flow at 10 mL/min) and the corresponding black and white image showing the area covered by the dye was used to reveal any pinning points in the coated tubes after flow. The piranha cleaned control displayed complete coverage by the dye whereas the layer 9 sample contained minimal pinning points.

Table SI1. Area covered by the blue dye in the glass tube. These values were used to generate the plot in Figure 8a.

	SiO_2-OH	**SiO_2-13F**	**1 LBL**	**5 LBL**	**9 LBL**
% Area Covered	98.286	79.556	16.092	0.382	0.014

Similarly, the center cross-section from each of the glass tubes in Figure 8b was cut out in equal dimensions as a representative portion of the entire tube. The images were processed using ImageJ to generate corresponding images in 8-bit grey scale. The software was used to produce a table tabulating the total area of the image, mean grey scale value, and

integrated density of each image (Table SI3). Background mean grey scale values were obtained from the top right non-fluorescent portion of Figure 8b (Table SI2). The following formula was used to generate the corrected total fluorescent values:
Total Fluorescence Intensity = Integrated Density – (Image area x Mean fluorescence of background readings). This technique[55] allows for quantification of the total image fluorescence and thus, degree of protein adhesion (Figure SI5). The plot in Figure 8b was used to generate these values. This technique was used as opposed to the above method for calculating the total area coverage because the threshold feature in ImageJ did not allow accurate control of coverage over the fluorescently illuminated areas.

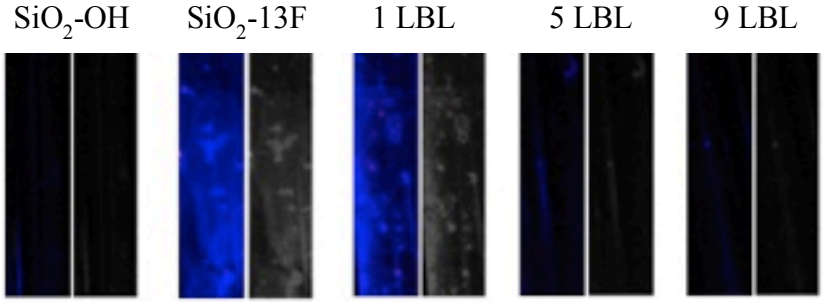

Figure SI5. Glass tubes were incubated with Alexa Fluor 350 conjugated streptavidin for 10 min (after 24 hours of water flow at 10 mL/min). A corresponding grey scale image was used to generate a histogram with the mean value indicating mean fluorescence intensity.

Table SI2: Background mean grey scale values were obtained from non-fluorescent sections of Figure 8b and then averaged. The final averaged mean value was used to generate the Corrected Total Fluorescence values in Table SI3.

Background	Area	Mean
1	1404	0.039
2	1512	0.078
4	1584	0.191
5	1170	0.076
Average		**0.096**

Table SI3: Tabulating the total area of the images, mean grey scale values, and integrated densities with the corresponding total fluorescence.

	Area	Mean	Integrated Density	Corrected Total Fluorescence
SiO_2-OH	21238	13.437	285373	283334.152
SiO_2-13F	22386	47.598	1065540	1063390.944
1 LBL	22308	43.172	963073	960931.432
5 LBL	22022	12.445	274058	271943.888
9 LBL	22308	13.952	311249	309107.432

5) Lubricant film thickness and shear stability

We compared the lubricant film thickness in samples prepared by calcination and by oxygen plasma treatment prior to silanization for both types of samples (after conditioning by vertical placement for 10 minutes) and for samples subjected to shear forces (using a spin-coating setup) to force lubricant out of the structures. The lubricant layer thickness was determined gravimetrically by measuring the weight of the samples before and after lubrication and

spinning at different rotational speeds consecutively for 1 min. Figure SI6 and Table SI4 show the measured lubricant thicknesses for the two types of samples as a function of the spinning speed. With increasing shear force, more lubricant is removed from the substrate. However, even at the highest spinning speed tested, the lubricant layer thickness (675 nm) was larger than the thickness of the coating (we used a coating of nine layers, with an approximate thickness of 100 nm), indicating that a lubricating film covering the nanostructures remained on the surface. Further, no differences between plasma treated and calcined samples were found, indicating comparable solid-lubricant interactions of the two different types of coating methods.

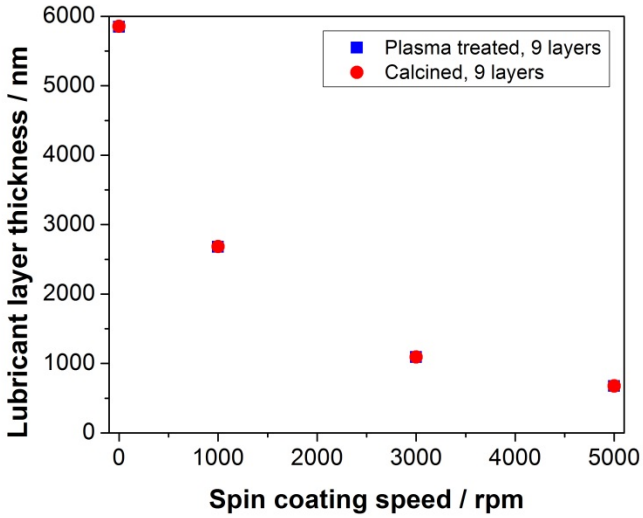

Figure SI6. Lubricant layer thickness as a function of spinning speed for samples prepared from calcination, acid piranha surface activation and silanization (red dots) and samples prepared from oxygen plasma surface activation and silanization (blue dots) *without* any calcination step.

Table SI4. Gravimetrical determination of the lubricant mass and layer thickness for samples before and after subjection to shear forces by spinning.

Spin speed /rpm	Lubricant weight /mg*cm^{-2}		Lubricant layer thickness / nm	
	plasma 9 player	calcined 9 layer	plasma 9 player	calcined 9 layer
0	1.09	1.09	5849	5859
1000	0.50	0.50	2680	2684
3000	0.20	0.20	1091	1092
5000	0.13	0.13	674	675

We then evaluated and compared the repellency performance of the lubricated samples prepared from calcination and plasma treatment after spincoating (Figure SI7) by measuring sliding angles of water and octane (10µl droplets). Both samples had a total number of nine deposited silica nanoparticle layers. Plasma treated and calcined samples showed similar repellency performance. The lubricated coatings maintained low octane sliding angles, even after spinning at 5000rpm. For water, a slight increase in sliding angles at elevated rotational

speeds was detected. However, the measured sliding angles of around 10° were still substantially smaller than for dry, fluorosilanized coatings (shown as dotted line in Figure SI7), indicating the presence of a thin lubricant layer after application of high shear forces.

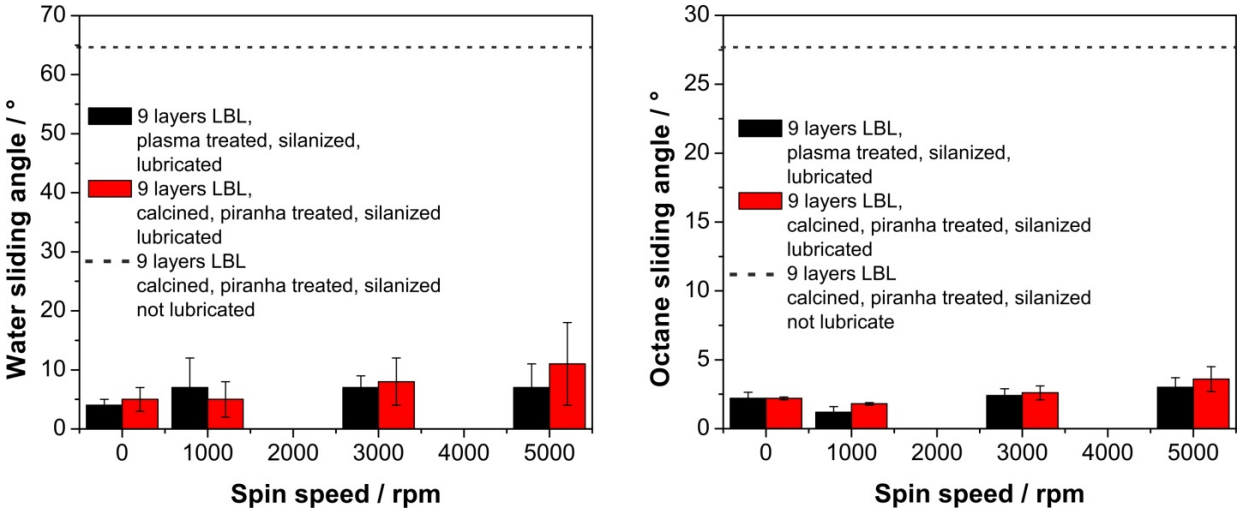

Figure SI7. Sliding angles of water and octane for substrates with 9 deposited silica nanoparticle layers for substrates prepared from 2 different methods before and after application of rotational shear forces performed in a spin-coater. *Calcined, piranha treated*, fluorosilanized and lubricated (red bars) as well as *oxygen plasma treated,* fluorosilanized and lubricated coatings (black bars) showed similar sliding angles for both water and octane. The dashed line shows sliding angles measured on coatings with a similar number of silica nanoparticle layers *without* application of the lubricant.

6) Layer-by-layer SLIPS coatings on different materials

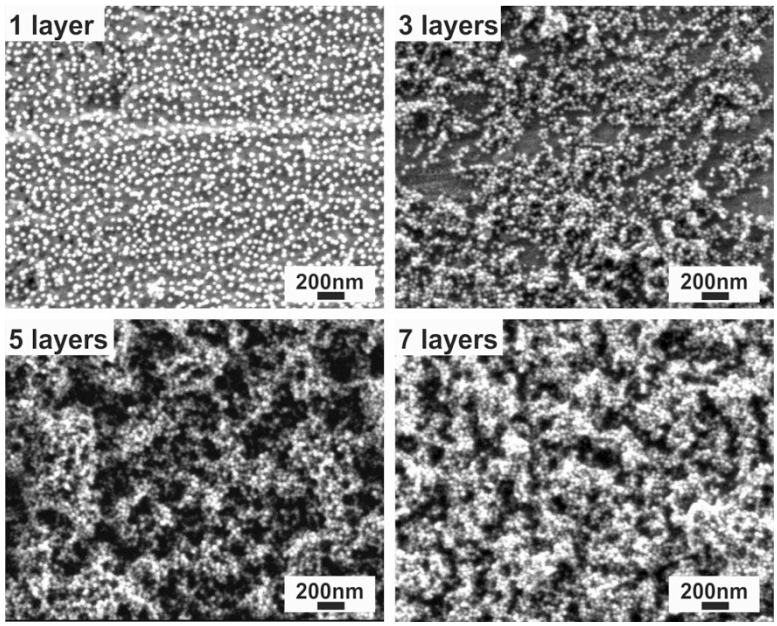

Figure SI8. SEM images of layer-by-layer coatings on aluminum with different deposition cycles.

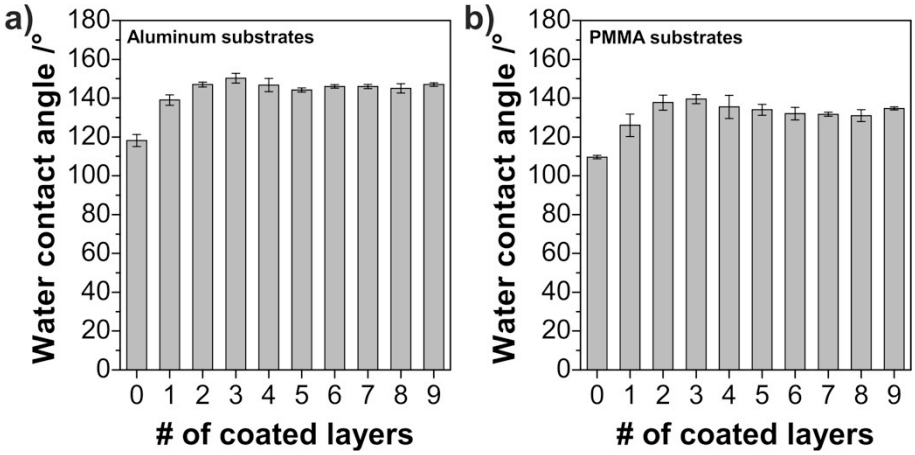

Figure SI9. Static contact angle of a 5 µl water droplet on aluminum (a) and poly(methylmethacrylate) (b) surfaces as a function of the number of deposited silica layers after oxygen plasma treatment (1min, 10sccm O, 100W) and silanization with (1H,1H,2H,2H-tetrahydrotridecafluorooctyl)-trichlorosilane.

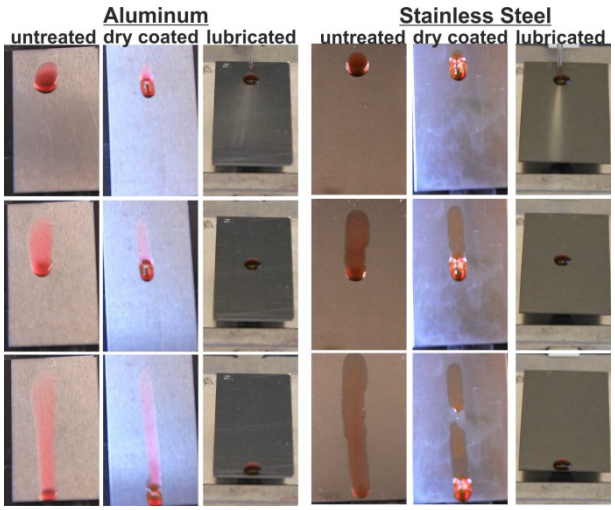

Figure SI 10a. Failure of untreated *metal* substrates (stainless steel and aluminum) and silica nanoparticle coated, fluorosilanized samples without addition of lubricant to repel stained octane. Effective repellency of octane without staining the surface is achieved only after infiltration of the coating with fluorinated lubricant.

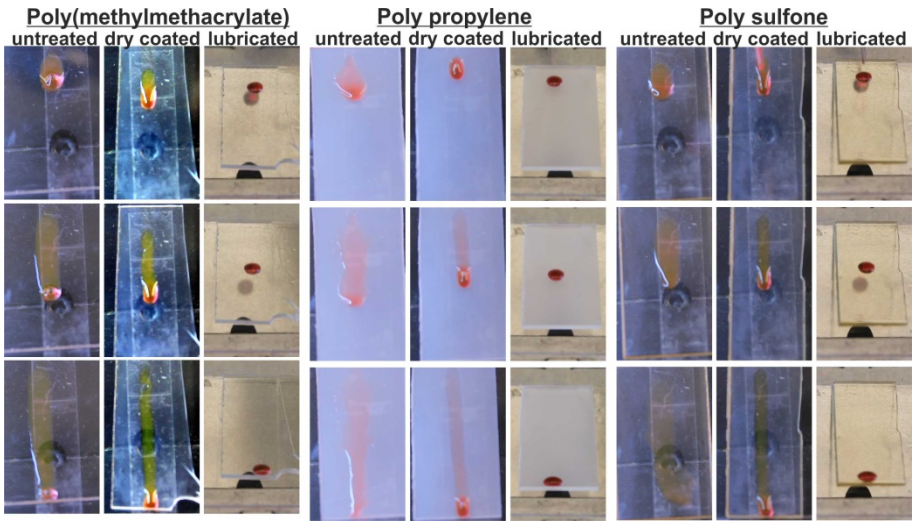

Figure SI 10b. Failure of untreated *polymer* substrates (poly-methyl methacrylate, poly propylene, poly sulfone) and silica nanoparticle coated, fluorosilanized samples without addition of lubricant to repel stained octane. Effective repellency of octane without staining the surface is achieved only after infiltration of the coating with fluorinated lubricant.

Table SI5. Dynamic contact angles of water on different substrates coated with a layer-by-layer silica nanoparticle coating (7 deposited layers).

Substrate Material	**Advancing/Receding contact angles /°**			**Contact angle hysteresis /°**		
	Uncoated	Dry coating	Lubricated coating	Uncoated	Dry coating	Lubricated coating
Glass	wetted	117±6/72±3	122±1/120±1	wetted	45±3	2±1
Aluminium	71±2/10±5	152±5/96±6	119±1/116±2	62±2	63±4	2±1
Stainless Steel	83±1/15±4	156±4/97±4	119±1/118±1	68±5	85±5	1±1
PMMA	90±2/45±3	128±8/77±13	119±1/119±1	45±3	51±15	1±1
PP	107±2/63±7	150±5/84±5	120±1/119±1	44±4	66±6	1±1
PSu	62±4/53±1	138±8/78±6	120±1/118±1	9±4	60±10	2±1

Table SI6. Dynamic contact angles of octane on different substrates coated with a layer-by-layer silica nanoparticle coating (7 deposited layers).

Substrate Material	**Advancing/Receding contact angles /°**			**Contact angle hysteresis /°**		
	Uncoated	Dry coating	Lubricated coating	Uncoated	Dry coating	Lubricated coating
Glass	wetted	62±1/21±6	50±1/49±1	wetted	41±6	1±1
Aluminium	wetted	63±2/11±3	51±2/49±1	wetted	51±4	2±1
Stainless Steel	wetted	64±2/12±3	52±1/51±2	wetted	52±4	1±1
PMMA	wetted	58±3/12±4	52±1/50±2	wetted	47±4	2±1
PP	wetted	58±3/11±3	52±1/51±1	wetted	48±6	1±1
PSu	wetted	62±1/10±1	53±1/51±1	wetted	44±5	2±1